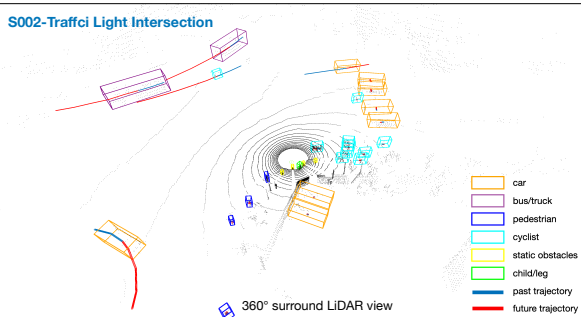


# 000 001 002 003 004 005 L4DOG: TOWARDS ROBUST BEV PERCEPTION FOR 006 QUADRUPED ROBOTS IN COMPLEX URBAN SCENES 007 008

009 **Anonymous authors**  
010  
011  
012  
013  
014  
015  
016  
017  
018  
019



020 Figure 1: We introduce L4Dog, the first large-scale BEV perception dataset for quadruped robots in  
021 complex urban environments. Featuring long-range perception in challenging scenarios, L4Dog provides  
022 high-quality manually annotated 3D ground truth and establishes benchmarks for multi-task BEV  
023 perception and occupancy prediction in 360°surrounding view.

## 024 ABSTRACT

025 Embodied intelligence in quadruped robots faces significant challenges in com-  
026 plex urban environments due to the limitations of traditional perception systems  
027 and the lack of comprehensive datasets for exteroceptive 3D perception. To ad-  
028 dress this, we introduce L4Dog, the first large-scale exteroceptive 3D perception  
029 dataset tailored for quadruped robots in open urban scenarios. L4Dog provides  
030 high-quality 360-degree surround-view sensor data and manual annotations, cov-  
031 ering diverse urban scenes such as traffic-light intersections, open roads, subway  
032 station, etc. By formulating perception tasks as bird’s-eye-view (BEV) space per-  
033 ception problems, we establish a multi-benchmark framework for BEV detection,  
034 tracking, trajectory prediction, and 3D traversable space occupancy estimation.  
035 The OmniBEV4D baseline method is proposed to unify multi-task perception  
036 (detection, tracking, prediction, and occupancy prediction) through shared tem-  
037 poral BEV features, enabling efficient and robust processing of dynamic urban  
038 environments. This work bridges the gap between current research and real-world  
039 deployment needs, offering a foundational resource for advancing autonomous  
040 navigation and decision-making in complex urban settings. The dataset will be  
041 made publicly available upon acceptance of this work.

## 042 INTRODUCTION

043 Embodied intelligence, as a pivotal research direction in artificial intelligence, is accelerating the de-  
044 ployment of advanced AI technologies on robotic platforms. Among these, quadruped robots have  
045 emerged as ideal mobile platforms due to their exceptional terrain adaptability, high mobility, and  
046 flexibility, demonstrating broad application potential in scenarios such as visually impaired assis-  
047 tance, elderly mobility support, and last-mile delivery services. However, their practical deployment  
048 in open urban road environments faces significant challenges: unlike controlled indoor or campus  
049 settings, real-world urban roads feature complex environments with diverse road types and heteroge-  
050 neous traffic participants (including pedestrians, vehicles, cyclists, static obstacles, etc.). Particularly  
051 under conditions of unpredictable traffic behaviors and highly dynamic environments, quadruped  
052 robots face heightened requirements for navigation planning, obstacle avoidance decisions, and in-  
053 teractive capabilities. Traditional forward-looking perception paradigms prove insufficient (Shah  
et al., 2021; 2022; Hirose et al., 2023), necessitating 360-degree surround-view and long-range

054 perception capabilities to identify fast-moving objects and enable evasive maneuvers; robustness  
 055 in densely crowded pedestrian scenarios and occluded visibility conditions within complex urban  
 056 areas must be enhanced; and critical advancements are required in establishing three-dimensional  
 057 semantic traversability understanding to address challenges posed by road surfaces, curbs, tactile  
 058 paving, and unknown obstacles.

059 As the core foundation for autonomous navigation and decision-making, perception systems in  
 060 quadruped robots are typically divided into two categories: proprioceptive and exteroceptive per-  
 061 ception (Miki et al., 2022). Proprioceptive perception focuses on processing sensor data from limb  
 062 joints, foot contacts, and inertial measurement units (IMUs) – such as joint encoders and foot con-  
 063 tact sensors – to estimate robot pose and control locomotion. Exteroceptive perception involves  
 064 acquiring and interpreting external environmental information for object recognition and interac-  
 065 tion. While extensive research in quadruped robotics has concentrated on terrain traversability op-  
 066 timization through proprioceptive enhancements (e.g., adaptability to varied terrains and parkour  
 067 capabilities) (Miki et al., 2022; Hoeller et al., 2024; Cheng et al., 2024; Fink & Semini, 2020; San-  
 068 tana et al., 2024; Lin et al., 2023; Lee et al., 2020; Shi et al., 2023), exteroceptive perception in  
 069 open-road scenarios remains critically underdeveloped: existing datasets are predominantly limited  
 070 to small-scale or indoor/campus environments with low complexity and insufficient data quality to  
 071 meet real-world urban road demands (Carlevaris et al., 2016; Yan et al., 2018; 2020; Hirose et al.,  
 072 2018; Martin et al., 2021; Karnan et al., 2022; Hirose et al., 2023; Wang et al., 2024; Zhang et al.,  
 073 2024; Luo et al., 2025). This pronounced gap between current research and future deployment needs  
 074 highlights the urgency of establishing exteroceptive perception benchmarks tailored for complex  
 075 urban environments.

076 Addressing this challenge, we present L4Dog, the first large-scale exteroceptive 3D perception  
 077 dataset for quadruped robots in complex urban scenarios. The "L4" designation borrows from  
 078 autonomous driving terminology, signifying level-4 autonomy in complex urban environments.  
 079 Equipped with high-specification sensors enabling full 360-degree surround-view coverage, L4Dog  
 080 surpasses existing quadruped datasets by encompassing challenging urban scenes including traffic-  
 081 light intersections, open roads, subway stations, and tactile paving areas, featuring complex human-  
 082 machine interaction scenarios with dense vehicle flows, pedestrians, and cyclists. We pioneer the  
 083 formulation of outdoor quadruped perception tasks as surround-view bird's-eye-view (BEV) per-  
 084 ception tasks, emphasizing three-dimensional BEV space perception for advanced autonomous nav-  
 085 igation and decision-making. Our dataset provides high-quality 3D manual annotations, establishing  
 086 multiple benchmark tasks including BEV detection, BEV tracking, and trajectory prediction. Fur-  
 087 thermore, we introduce the first occupancy grid representation for 3D traversable space in quadruped  
 088 robotics, with manual annotations of 360-degree occupancy grids surrounding the robot, thereby  
 089 proposing the inaugural occupancy benchmark in exteroceptive perception for quadruped platforms.  
 090 For multi-task perception (detection, tracking, prediction, occupancy prediction), we propose the  
 091 OmniBEV4D baseline method, which formalizes exteroceptive tasks as BEV perception tasks and  
 092 supports multi-task perception capabilities.

093 Our core contributions are summarized as follows:

- 094 1) We introduce L4Dog, the first BEV perception dataset for quadruped robots in open complex  
 095 urban scenarios, featuring high-quality manual annotations. This work pioneers the formulation of  
 096 quadruped exteroceptive 3D perception as a fused BEV-space perception task.
- 097 2) We establish a multi-benchmark framework for BEV environmental perception in quadruped  
 098 robots, encompassing challenging tasks in BEV object detection, multi-target tracking, and trajec-  
 099 tory prediction.
- 100 3) We propose the first occupancy network prediction framework for 360-degree 3D traversable  
 101 space in quadruped robots, accompanied by high-quality occupancy annotations.
- 102 4) We develop the OmniBEV4D perception framework, which leverages shared temporal BEV fea-  
 103 tures through a multi-task architecture to simultaneously enable BEV perception, tracking, trajectory  
 104 prediction, and occupancy estimation, serving as the baseline method for L4Dog benchmark tasks.

105 The remainder of this paper is organized as follows: Section 2 reviews related datasets and perception  
 106 methodologies in quadruped robotics; Section 3 details the L4Dog dataset; Section 4 presents the  
 107

108 multi-perception benchmarks and the OmniBEV4D baseline; Section 5 concludes with future work  
 109 perspectives.  
 110

## 111 2 RELATED WORK

### 112 2.1 QUADRUPED ROBOT PERCEPTION DATASETS

114 Quadruped robot perception datasets can be categorized into proprioception (locomotion-focused)  
 115 and exteroception (environmental understanding) types (Miki et al., 2022). This work focuses on  
 116 exteroception, typically employing optical sensors such as RGB cameras, RGB-D cameras, and  
 117 LiDAR. Notable datasets include SCAND (Karnan et al., 2022), which equipped ClearPath Jackal  
 118 and Spot robots with 16-beam LiDAR and stereo RGB cameras to collect teleoperated traversal  
 119 data for social navigation; NCLT (Carlevaris et al., 2016), which provides long-term campus data  
 120 with 32-beam LiDAR and omnidirectional cameras for mapping applications; and RECON (Shah  
 121 et al., 2021), ViKing (Shah et al., 2022), and GND (Liang et al., 2024), which serve as general-  
 122 purpose mapping datasets. Specialized traversability datasets include ForestTrav (Ruetz et al., 2024),  
 123 TRIP (Oh et al., 2024), and GoStanford (Hirose et al., 2018) for outdoor and indoor environments.  
 124 Crucially, none of these datasets include explicit object recognition (e.g., pedestrian detection) or  
 125 provide supervised annotations.  
 126

127 For explicit quadruped perception, FLOBOT (Yan et al., 2020) provides indoor pedestrian annotations  
 128 using 16-beam LiDAR and stereo RGB-D cameras, while L-CAS (Yan et al., 2018) offers 3D  
 129 pedestrian annotations in office environments with 16-beam LiDAR. QuadTrack (Luo et al., 2025)  
 130 focuses on 2D multi-frame pedestrian tracking with panoramic cameras, and TBD Pedestrian (Wang  
 131 et al., 2024) provides indoor pedestrian tracking with 3D annotations from single-beam LiDAR. Re-  
 132 cent large-scale pedestrian datasets include JRDB (Martin et al., 2021), SiT (Bae et al., 2023), and  
 133 CODa (Zhang et al., 2024), which feature varying sensor configurations with extensive 3D annota-  
 134 tions.  
 135

136 Our work (L4Dog) belongs to explicit supervised quadruped perception, sharing similarities with  
 137 (Bae et al., 2023), (Martin et al., 2021), and (Zhang et al., 2024) but introducing five key innova-  
 138 tions. First, it represents the largest 3D-annotated quadruped exteroception dataset, being an order  
 139 of magnitude larger than JRDB/CODa. Second, it captures Level 4 complex urban environments  
 140 with high object density. Third, it pioneers the formulation of quadruped exteroception as 360°BEV  
 141 perception. Fourth, it provides additional 3D occupancy annotations for traversable space. Please  
 142 refer to Table 1 for a comprehensive comparison of exteroception datasets.  
 143

### 144 2.2 QUADRUPED ROBOT PERCEPTION METHODS

145 As stated, this work focuses on quadruped exteroception tasks; proprioceptive methods for loco-  
 146 motion are omitted. Exteroceptive methods primarily evaluate environmental traversability for nav-  
 147 igation and interaction, divided into terrain recognition and object recognition. Terrain recognition  
 148 classifies ground surfaces to assess traversability, while object recognition detects obstacles (e.g.,  
 149 pedestrians, traffic cones) in 2D/3D space. Representative approaches include FLOBOT’s SVM  
 150 and Bayesian tracking (Yan et al., 2020), TBD Pedestrian’s ByteTrack-based 2D tracking (Wang  
 151 et al., 2024), L-CAS’s LiDAR clustering with UKF tracking and SVM classification (Yan et al.,  
 152 2018), JRDB’s YoloV3/RetinaNet for 2D detection and Frustum PointNet for 3D detection (Mar-  
 153 tin et al., 2021), and SiT/CODa’s LiDAR-based detectors (FCOS3D/PointPillar/CenterPoint) (Bae  
 154 et al., 2023; Zhang et al., 2024).  
 155

156 Given L4Dog’s focus on exteroception in complex urban roads with dense traffic, we adopt au-  
 157 tonomous driving paradigms by formulating quadruped exteroception as Bird’s-Eye-View (BEV)  
 158 perception. Our technical approach combines whitelist-based BEV recognition and non-whitelist  
 159 occupancy recognition methods.  
 160

### 161 2.3 BEV PERCEPTION IN AUTONOMOUS DRIVING

162 BEV perception has experienced significant advancements in the field of autonomous driving in re-  
 163 cent years. The core concept involves mapping multi-sensor data through coordinate transformation  
 164 to unify features in the BEV space for representation and learning. Representative works for BEV  
 165 detection include LSS (Phlion & Fidler, 2020), BEVFormer (Li et al., 2022), BEVDet (Huang  
 166 et al., 2021), and BEVFusion (Liu et al., 2022). Occupancy Prediction, a novel benchmarking task  
 167

162  
 163  
 164  
 165  
 Table 1: Comparison of exteroception datasets for (quadruped) robots. L4Dog supports 360-degree  
 panoramic sensor fusion recognition, outperforming SOTA benchmarks in data scale, 3D object  
 annotation capacity, and object density. L4Dog enables multi-modal external perception tasks in-  
 cluding BEV perception, trajectory prediction, and occupancy prediction.

166	Dataset	Published	Num Samples/ Duration	Scene	360° L+C/ Obj Density/ 3D objs	Exteroception Tasks	Sensors
168	NCLT Carlevaris et al. (2016)	IJRR IF 5.0	N/A 34.9 h	indoor outdoor campus	✓ N/A 0	N/A	32&2-beam LiDAR 360° Camera
170	L-CAS Yan et al. (2018)	IROS	28,002 0.82 h	indoor office	✗ 1,12 6,140	Human Detection & Tracking	16-Beam LiDAR N/A
172	GoStanford Hirose et al. (2018)	IROS	10,560 N/A	indoor office	✗ N/A 0	2D Traversable Probability	360° RGB Camera N/A
174	FLOBOT Yan et al. (2020)	ISR IF 4.3	16,570 0.46 h	indoor airport etc.	✗ N/A 968	Human Detection & Tracking	16-Beam & 2D-LiDAR RGB-D Stereo
176	RECON Shah et al. (2021)	arXiv	5,000 N/A	outdoor 9 sites	✗ N/A 0	N/A	2D LiDAR Stereo Camera
178	JRDB Martin et al. (2021)	TPAMI IF 20.8	60,000 1.07 h	indoor outdoor campus	✓ 30 1.8 million	Human Detection & Tracking	2x 16-Beam LiDAR Stereo & Fisheye Camera
180	SCAND Karnan et al. (2022)	RA-L IF 5.3	N/A 8.7 h	indoor outdoor campus	✓ N/A 0	N/A	16-Beam LiDAR RGB-D & surround RGB
182	Seattle Shaban et al. (2022)	CoRL	N/A 1 h	outdoor offroad	✗ N/A 0	LiDAR Semantic segmentation	64-Beam LiDAR
184	ViKiNG Shah et al. (2022)	RSS	N/A 12 h	outdoor sidewalks/parks	✗ N/A 0	N/A	N/A 170° RGB Camera
186	SACSoN Hirose et al. (2023)	RA-L IF 5.3	N/A 75 h	indoor office	✗ N/A 0	N/A	2D LiDAR Spherical RGBD
188	SiT Bae et al. (2023)	NeurIPS	12,000 0.33 h	indoor outdoor Open Scenes	✓ 26.7 0.32 million	Human Detection, Tracking, Prediction	2x 16-Beam LiDAR 5x Camera
190	ForestTrav Ruetz et al. (2024)	IEEE Access IF 3.6	N/A N/A	outdoor forest	✓ N/A 0	probabilistic 3D voxel map	16-Beam LiDAR/ 4x RGB Camera
192	CEAR Zhu et al. (2024)	RA-L IF 5.3	N/A N/A	indoor outdoor	✗ N/A 0	N/A	16-Beam LiDAR/ Event&RGBD Camera
194	TBD Pedestrian Wang et al. (2024)	ICRA IF 4.55	N/A 3.55 h	indoor Mall	✓ N/A 11,716	Human Tracking	3D-LiDAR/ 360°&Stereo Camera
196	CODa Zhang et al. (2024)	T-RO IF 10.5	34,800 1 h	indoor outdoor campus	✗ 37.4 1.3 million	LiDAR 3D Detection	128-Beam LiDAR/ 2xRGB&RGBD Camera
198	QuadTrack Luo et al. (2025)	CVPR	19,000 0.5 h	outdoor campus	✗ 9.89 0.19 million	2D mot	N/A/ Panoramic Camera
200	L4Dog(ours)	2025	360,000 10 h	outdoor complex urban	✓ 48.7 17.5 million	BEV Detection & Tracking Trajectory Prediction Occupancy Prediction	32-Beam LiDAR/ 5x RGB Camera

200  
 201  
 202  
 203  
 204  
 205  
 206  
 207  
 208  
 209  
 introduced in autonomous driving, addresses the challenge of detecting non-standard obstacles by  
 representing 3D space through a voxelized grid. Notable approaches include Occ3D (Tian et al.,  
 2023), OpenOcc (Tong et al., 2023), SparseOcc (Liu et al., 2023), FBOcc (Li et al., 2023), and  
 FlashOcc (Yu et al., 2023). This work builds on autonomous driving’s BEV paradigm by introduc-  
 ing the first first-person BEV perception methodology for quadrupedal robots. The data distribu-  
 tion, scene complexity, and object representation challenges in this context differ significantly from  
 autonomous driving, offering unique value for quadrupedal robotics. Beyond BEV detection and  
 occupancy prediction, we propose BEV tracking and trajectory prediction tasks, introducing four  
 novel external perception benchmarks tailored for quadrupedal robots. Finally, we introduce the first  
 multi-task BEV recognition framework integrating all four benchmarks.

### 210 3 DATASET

#### 211 3.1 PLATFORM & SENSORS

213  
 214  
 215  
 We selected a quadruped robotic dog as our data acquisition platform. Compared to alternative mo-  
 bile robotic platforms (e.g., Clear Path robots), legged systems offer superior terrain adaptability,  
 enhanced mobility, and greater commercialization potential. Specifically, to address diverse urban  
 scenarios including sidewalks, roadways, and tactile paving (Section 3.3), we employed the wheeled

216  
217  
218  
219  
220  
221  
222  
223  
224  
225  
226  
227  
228  
229

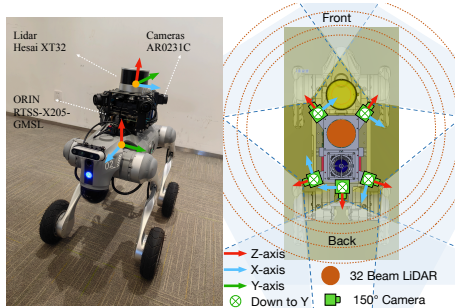


Figure 2: Sensor Setup on Unitree Go2. One 32-beam LiDAR and five 150°-FOV cameras. Blue: camera FoV; brown dots: LiDAR coverage.

quadruped Unitree Go2 (Unitree, 2025-07-27) as the L4Dog acquisition platform. This hybrid locomotion system enables wheeled movement on flat surfaces and legged locomotion on uneven terrain (e.g., tactile paving) and elevation changes (curbs), demonstrating exceptional terrain traversal capabilities. For obstacle avoidance (vehicles, motorcycles, pedestrians, static obstacles) during urban navigation, precise 3D object recognition is essential.

Consequently, a high-performance 360° perception system was implemented, comprising one 32-beam LiDAR and five RGB cameras to provide fused point cloud and visual data. Compared to 16-beam LiDARs (Table 1), the 32-beam configuration yields higher point density and extended detection range. Unlike RGB-D or stereo cameras, the multi-camera panoramic system delivers comprehensive 360° visual coverage that spatially aligns with LiDAR point clouds, enriching 3D data with semantic information. Relative to panoramic cameras, this multi-camera configuration achieves superior detection range and reduced image distortion. The 360° LiDAR-camera fusion approach follows autonomous driving paradigms (nuScenes (Caesar et al., 2020), nuPlan (Caesar et al., 2021), Waymo (Sun et al., 2020), PandaSet (Xiao et al., 2021), Argoverse (Wilson et al., 2023)), addressing L4 perception challenges in complex pedestrian/vehicle environments while supporting BEV perception formulations. Wide-angle RGB cameras were mounted vertically (90° rotation) to maintain 360° coverage while expanding vertical perception. This configuration ensures full-body imaging of nearby pedestrians (0.4m). Sensor specifications are listed in Table 2.

### 3.2 COORDINATES, CALIBRATION AND SYNCHRONIZATION

#### 3.2.1 COORDINATE SYSTEMS

The L4Dog platform employs five coordinate systems for spatial perception and sensor fusion Figure 2, including image UV coordinates for 2D pixel representation in vision data, camera coordinates as a 3D frame centered at the optical axis for geometric transformations, IMU coordinates aligned with inertial sensor axes for motion state estimation, LiDAR coordinates for high-resolution 3D point cloud mapping, and robot coordinates as a body-fixed frame for navigation and control. These coordinate systems are synergistically integrated through transformation matrices, with cross-sensor calibration achieved via the following methods.

#### 3.2.2 CALIBRATION PROCEDURES

- **Cameras:** Calibrated using checkerboard patterns and pinhole camera models to establish image-to-camera coordinate transformations (Zhang, 1999).
- **Camera-to-LiDAR:** Extrinsic calibration performed pairwise, with projection matrices optimized until static point cloud projections achieved pixel-level alignment.
- **IMU-to-Robot:** Transformation derived from measured installation offsets and angles.
- **LiDAR Motion Compensation:** IMU motion estimates applied for dynamic point cloud distortion correction.
- **LiDAR-to-IMU:** LiDAR-to-IMU calibration is initialized using CAD drawings and on-site installation measurements, and further refined via the LI-Init calibration method (Zhu et al., 2022).

Table 2: Sensor Specifications. We utilize 5 x cameras and 1 x LiDAR deployed in a 360° configuration. IMU uses the built-in IMU of the robotic dog.

Sensor	Num	Specifications
Camera	5	RGB image @ 1920x1080 resolution, 10Hz, FOV=150°.
LiDAR-32	1	Spinning, 32 beams, 10Hz, 360°×31FOV @ 0.18°×1 resolution, 0.05–120m range @ $\pm 0.5\text{cm}$ accuracy, with up to 6.4M points per second.

Table 3: Data collection scenes statistics.

Scene ID	Scene	Clips	Annotated Objects	Features
S001	Subway	363	1.93M	dense pedestrians
S002	Traffic light intersections	1798	10.3M	complex traffic flow
S003	Open Road	1081	3.5M	mix of pedestrians and vehicles
S004	Tactile Paving	358	1.75M	narrowly passable

### 3.2.3 SYNCHRONIZATION

All sensors were synchronized via a high-precision Precision Time Protocol (PTP) server, with timestamps referenced to the LiDAR’s timestamp. Camera exposure triggers were initiated at LiDAR scan center alignment, defining camera timestamps. LiDAR timestamps marked completion of full rotational scans, with motion compensation applied using localization data to account for scan duration.

## 3.3 DATA COLLECTION SCENES AND COLLECTION PLANS

L4Dog focuses on first-person 3D perception datasets for quadruped robots operating in complex urban environments. The data was collected during peak hours in four distinct urban scenarios (Table 3): 1) Subway stations, characterized by high pedestrian density and dynamic interactions between people and non-motorized vehicles; 2) Traffic light intersections involving complex interactions between vehicles and pedestrians; 3) Open roads with mixed vehicle/non-motorized traffic; 4) Tactile paving areas with narrow space, requiring specialized navigation for assistive applications. Representative annotated samples are visualized in Figure 4.

## 3.4 GROUND TRUTH FORMATS AND ANNOTATION

As previously formulated, perception tasks are structured as BEV problems comprising: 1) BEV 3D detection ground truth for whitelisted objects; and 2) 3D traversability (occupancy) ground truth for non-whitelisted entities.

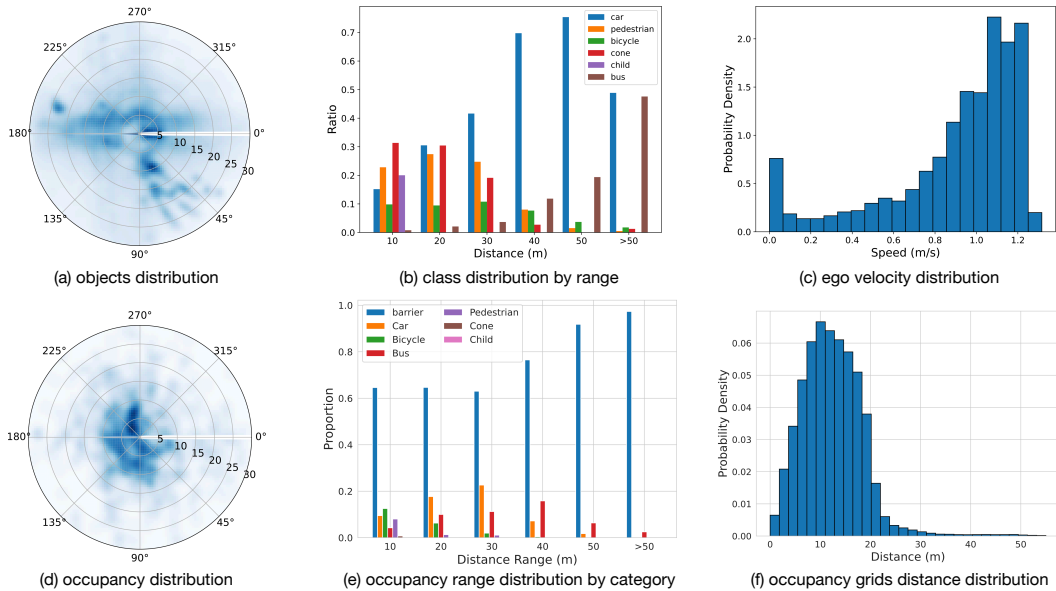


Figure 3: L4Dog Dataset Statistics: (a) 360° heatmap of object distribution relative to the ego robot. (b) Object category distribution by distance from the ego robot. (c) Ego robot speed distribution. (d) 360° heatmap of occupancy grid distribution relative to the ego robot. (e) Occupancy category distribution by distance from the ego robot. (f) Occupancy grid distance distribution. Note "child" and "leg" are treated as interchangeable terms for the same category.

324 3.4.1 BEV 3D OBJECT ANNOTATION  
325

326 Each sensor frame was manually annotated for whitelisted objects within 50m. Annotations include  
327 3D bounding boxes parameterized as ( $id$ ,  $cls$ ,  $x$ ,  $y$ ,  $z$ ,  $w$ ,  $l$ ,  $h$ , yaw), where:  $id$  denotes unique object  
328 identifiers enabling tracking/prediction across 10Hz frames (100ms intervals);  $cls$  indicates object  
329 category  $\in \{\text{car, bus/truck, pedestrian, cyclist, static obstacle, legs/child}\}$ ; ( $x$ ,  $y$ ,  $z$ ) specifies robot-  
330 centric coordinates (meters); ( $w$ ,  $l$ ,  $h$ ) defines physical dimensions (meters); and yaw defines the  
331 heading angle. Notably, 'legs' category denotes pedestrians within 0.4m where upper-body occlu-  
332 sion prevents full-body detection. Annotations were performed using a custom LiDAR-RGB fusion  
333 tool, primarily labeling 3D boxes in point clouds with image projection validation. All annotations  
334 underwent secondary quality assurance, achieving  $\geq 98\%$  accuracy.

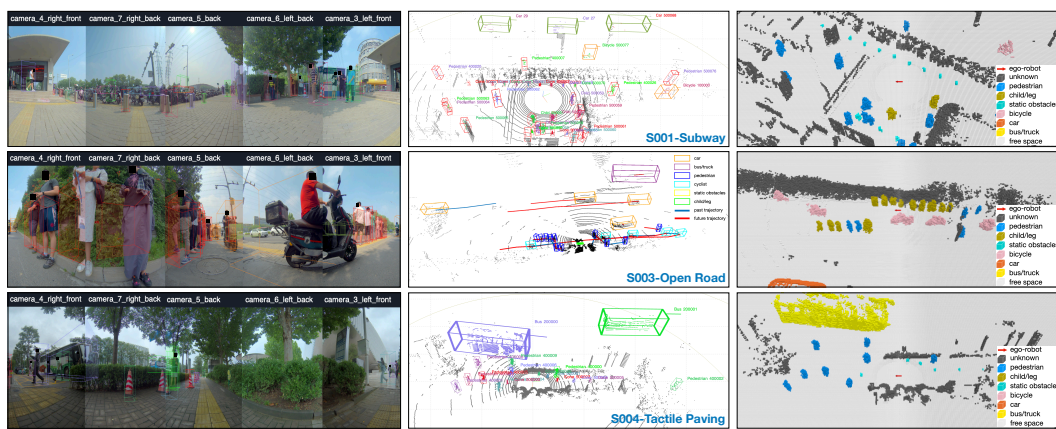
335 3.4.2 3D OCCUPANCY GRID ANNOTATION  
336

337 Beyond dynamic object perception, L4Dog addresses non-whitelisted object recognition and 3D  
338 traversability estimation (e.g., curb negotiation, obstacle avoidance). Departing from elevation map  
339 representations ( (Miki et al., 2022)), we formulate this as 3D occupancy estimation, encoded as  $cls$ ,  
340  $x$ ,  $y$ ,  $z$ ,  $grid\_size$  to resolve traversability and open-set recognition.

341 Occupancy ground truth generation adapts autonomous driving methodologies (Tian et al., 2023;  
342 Tong et al., 2023): 1) Dynamic objects (Section 3.4.1 annotations) are transformed to object-centric  
343 coordinates for multi-frame point cloud accumulation; 2) After temporal reconstruction and motion  
344 compensation, static backgrounds are processed via multi-frame point cloud fusion and mesh recon-  
345 struction; 3) Ground planes (relative traversable surfaces) are segmented and removed; 4) Remaining  
346 point clouds are voxelized ( $grid\_size=0.2m$ ) within a cylindrical volume (radius=50m, height=[-  
347 1m, 4m], robot-centric), into 8 categories (besides bbox categories, add free space and unknown).  
348 The ground truth labels underwent a final round of manual quality control and refinement. Occupa-  
349 ncy representations are illustrated in Figure 1.

350 3.5 STATISTICAL ANALYSIS  
351

352 Dataset statistics are presented in Figure 3, where we analyze the distribution of objects and occu-  
353 pancy grids under the ego robot. The analysis includes heat map distributions, category distributions  
354 within 10-meter intervals, distance distributions, and velocity distributions during robot data col-  
355 lection. As shown in the figure, L4Dog exhibits characteristics such as complex multi-class object  
356 distributions, long-range objects, and high-density occupancy grids.



357  
358 Figure 4: More collection scenes and GT illustration samples for each scene. For S002 traffic-light  
359 intersection please refer to Figure 1. From left to right: Cameras, LiDAR, Occupancy. We showcase  
360 detection & tracking frame in S001 and S004, motion frame in S003.  
361  
362

363 3.6 PRIVACY PROTECTION  
364

365 All human faces and license plates in image data were anonymized using mosaic blurring to ensure  
366 privacy and data security.

## 378 4 BENCHMARKING & BASELINES

380 We introduce two core benchmarks on the L4Dog dataset: BEV Object Recognition (Section 4.1)  
 381 and Occupancy Prediction (Section 4.2). The BEV Object Recognition benchmark encompasses  
 382 three subtasks: BEV Object Detection (Section 4.1.1), BEV Object Tracking (Section 4.1.2), and  
 383 Object Trajectory Prediction (Section 4.1.3). Furthermore, we propose a multitask baseline frame-  
 384 work that enables simultaneous performance of all four perception tasks through a unified neural  
 385 network architecture (Section 4.3). Notably, L4Dog represents the first and only work in quadruped  
 386 robotics perception research to systematically establish benchmarks for both BEV object recognition  
 387 and occupancy prediction.

### 388 4.1 BEV OBJECT RECOGNITION

#### 389 4.1.1 BEV OBJECT DETECTION

390 Task Description: Analogous to BEV detection in autonomous driving research, L4Dog’s BEV  
 391 object detection aims to identify object categories, positions, orientations, and dimensions within  
 392 the robot’s 360° surroundings using LiDAR and surround-view images. Distinct from auto-  
 393 motive applications, L4Dog presents algorithmic challenges including dense non-rigid objects,  
 394 severe pedestrian occlusion, and partial observation of pedestrians (leg categories) from the  
 395 robot’s low vantage point. The formulation is expressed as:  $(cls, conf, x, y, z, w, l, h, yaw) = \mathcal{F}((I_0, I_1, I_2, I_3, I_4), L, t)$  where  $I_i$  denotes JPEG images from five cameras,  $L$  represents Li-  
 396 DAR point clouds (PCD format), and  $t$  indicates the temporal component (optional for single-frame  
 397 detection; required for 4D multi-frame detection). The outputs include object class ( $cls$ ), confidence  
 398 ( $conf$ ), position ( $x, y, z$ ), bounding box dimensions ( $w, l, h$ ), and yaw angle. For evaluation, we  
 399 employ widely used mAP as the metric:  $mAP = \frac{1}{N} \sum_{c=1}^N \left( \frac{1}{11} \sum_{r \in \{0, 0.1, \dots, 1\}} \max_{\tilde{r} \geq r} p_c(\tilde{r}) \right)$ .

#### 402 4.1.2 BEV OBJECT TRACKING

403 Task Description: This task focuses on associating unique IDs to detected objects across consecutive  
 404 frames. By integrating object detection,  
 405 motion modeling, and data association  
 406 techniques, it addresses challenges such  
 407 as target occlusion and background  
 408 interference. The benchmark supports  
 409 both two-stage *tracking-by-detection*  
 410 and one-stage *tracking-by-learning*  
 411 paradigms. BEV object tracking further  
 412 enables downstream functionalities  
 413 including velocity/acceleration es-  
 414 timation and trajectory prediction.  
 415 Performance is evaluated using MOTA:  

$$MOTA = 1 - \frac{\sum_t (FP_t + FN_t + IDSW_t)}{\sum_t GT_t}$$
.

#### 418 4.1.3 419 OBJECT TRAJECTORY PREDICTION

420 Task Description: This component pre-  
 421 dicted future motion trajectories of  
 422 objects based on their historical move-  
 423 ments (using Track IDs). Implemen-  
 424 tations may follow either two-stage  
 425 *prediction-by-observation* or one-stage  
 426 *learning-based* approaches. Quantitative  
 427 assessment uses ADE and FDE metrics:  $ADE = \frac{1}{T \cdot N} \sum_{i=1}^N \sum_{t=1}^T \left\| \hat{\mathbf{p}}_t^{(i)} - \mathbf{p}_t^{(i)} \right\|$ ,  $FDE = \frac{1}{N} \sum_{i=1}^N \left\| \hat{\mathbf{p}}_T^{(i)} - \mathbf{p}_T^{(i)} \right\|$ .

#### 428 4.2 OCCUPANCY PREDICTION

430 Task Description: This task predicts 3D spatial occupancy within the robot’s sensing range to deter-  
 431 mine navigable areas. We discretize a cylindrical volume (radius: 50m; height: [-1m, 4m]) centered  
 432 on the robot into grids (grid\_size = 0.2m). Similar to autonomous driving formulations, each grid

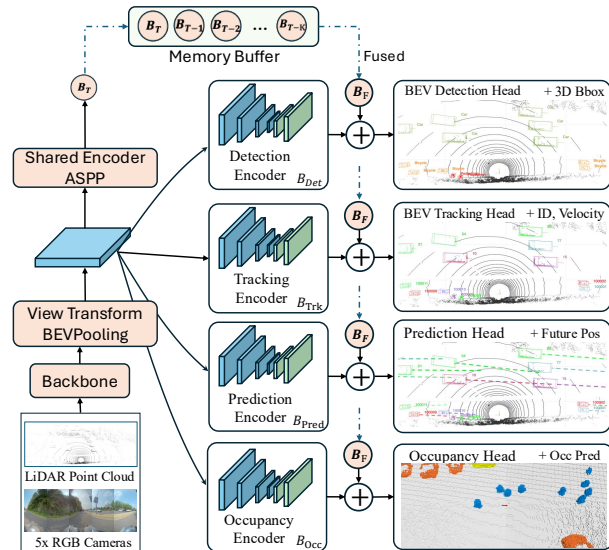


Figure 5: OmniBEV4D: Multitasking Baseline Method

432 is characterized by  $\{\text{cls}, \text{conf}, x, y, z, \text{occupied}\}$ , where  $\text{cls}$  denotes category,  $\text{conf}$  indicates confidence,  $(x, y, z)$  represents robot-centric coordinates, and  $\text{occupied}$  is a binary occupancy flag. We  
 433 utilize mIoU (Tian et al., 2023) and RayIoU (Liu et al., 2023) as metrics. mIoU measures voxel-  
 434 wise overlap between predicted and ground-truth occupancies, while RayIoU evaluates occupancy  
 435 consistency along sensor rays by comparing predicted and actual ray termination points.  
 436

### 437 4.3 METHOD & EXPERIMENTS

#### 438 4.3.1 BASELINE METHOD: OMNIBEV4D

440 A naive baseline approach would apply classical methods (e.g., BEVDet (Huang et al., 2021) for  
 441 detection, ByteTrack (Zhang et al., 2022) for tracking) independently to each task. However, we  
 442 contend that such single-task baselines offer limited value for L4Dog’s complex scenarios, as no  
 443 individual task suffices for quadruped robots’ navigation requirements.

444 Moreover, combining four separate baselines incurs significant computational redundancy, precluding  
 445 real-time deployment. Therefore, we propose OmniBEV4D—a strong multitasking baseline for  
 446 L4Dog perception. As illustrated in Figure 5, this LiDAR-camera fusion network maximizes com-  
 447 putational sharing through: 1) joint feature extraction from heterogeneous sensors, 2) unified feature  
 448 fusion, and 3) shared 4D memory buffer. Task-specific heads then branch for BEV detection, track-  
 449 ing, trajectory prediction, and occupancy estimation.

#### 450 4.3.2 L4DOG EXPERIMENTS & ABLATIONS

451 We conduct quantitative evaluations of OmniBEV4D on the L4Dog dataset, presenting compara-  
 452 tive results against classical quadruped exteroceptive methods across the proposed tasks (see Ta-  
 453 ble 4). As demonstrated, OmniBEV4D achieves state-of-the-art performance while handling mul-  
 454 tiple tasks. Furthermore, we conducted ablation studies by training OmniBEV4D on nuScenes and  
 455 CODa datasets, followed by evaluation on L4Dog. The performance degradation observed highlights  
 456 the distinct distribution and complexity characteristics of our proposed L4Dog dataset.

457 Table 4: Quantitative Evaluation on L4Dog.  
 458

459 Methods	460 BEVDet mAP $\uparrow$	461 BEVTrk MOTA $\uparrow$	462 TrajPred ADE/FDE $\downarrow$	463 OccPred mIoU/RayIoU $\uparrow$
464 PointPillar (Lang et al., 2019)	58.4%	—	—	—
465 BEVFusion (Liu et al., 2022)	70.1%	—	—	—
466 ByteTrack (Zhang et al., 2023)	—	57.9%	—	—
467 GANet (Wang et al., 2022)	—	—	1.24/2.16	—
468 FBOcc (Li et al., 2023)	—	—	—	48.5%/43.2%
469 OmniBEV4D-nuScenes	52.4%	58.3%	1.45/1.98	33.2%/36.4%
470 OmniBEV4D-CODa	60.3%	—	—	—
471 OmniBEV4D (ours)	70.4%	65.4%	1.24/1.76	45.6%/52.4%

## 472 5 CONCLUSION & FUTURE WORK

473 We present L4Dog, the largest and most complex exteroceptive perception dataset to date in  
 474 quadruped robotics research. L4Dog encompasses temporally continuous multi-modal sensor data  
 475 and human-annotated ground truth across complex urban scenarios including subway stations, traf-  
 476 fic intersections, and open roads. This work pioneers the formulation of quadruped robotic per-  
 477 ception as BEV tasks, establishing comprehensive benchmarks for BEV detection, BEV tracking,  
 478 and trajectory prediction. Furthermore, we introduce the first occupancy prediction benchmark with  
 479 corresponding ground truth for quadruped robots.

480 To address the multitasking requirements of practical autonomous navigation, we propose Omni-  
 481 BEV4D—a unified framework that simultaneously generates inference results for all perception  
 482 tasks through shared spatiotemporal feature computation. Quantitative evaluations on the L4Dog  
 483 dataset validate the effectiveness of the OmniBEV4D approach, with ablation studies highlighting  
 484 the dataset’s value.

485 Future work will incorporate natural language annotations to support Vision-Language Models  
 486 (VLM) and Visual Question Answering (VQA) research, navigation trajectory recordings for Vision-  
 487 and-Language Navigation (VLN) studies, and low-level control signal acquisition to enable Vision-  
 488 Language-Action (VLA) research.

486 REFERENCES  
487

488 Jong Wook Bae, Jungho Kim, Junyong Yun, Changwon Kang, Jeongseon Choi, Chanhyeok Kim, Junho Lee,  
489 Jungwook Choi, and Jun Won Choi. Sit dataset: socially interactive pedestrian trajectory dataset for social  
490 navigation robots. *Advances in neural information processing systems*, 36:24552–24563, 2023.

491 Holger Caesar, Varun Bankiti, Alex H Lang, Sourabh Vora, Venice Erin Liang, Qiang Xu, Anush Krishnan,  
492 Yu Pan, Giancarlo Baldan, and Oscar Beijbom. nuscenes: A multimodal dataset for autonomous driving.  
493 In *Proceedings of the IEEE/CVF conference on computer vision and pattern recognition*, pp. 11621–11631,  
494 2020.

495 Holger Caesar, Juraj Kabzan, Kok Seang Tan, Whye Kit Fong, Eric Wolff, Alex Lang, Luke Fletcher, Oscar  
496 Beijbom, and Sammy Omari. nuplan: A closed-loop ml-based planning benchmark for autonomous vehicles.  
497 *arXiv preprint arXiv:2106.11810*, 2021.

498 Carlevaris, Nicholas, Arash K Ushani, and Ryan M Eustice. University of michigan north campus long-term  
499 vision and lidar dataset. *The International Journal of Robotics Research*, 35(9):1023–1035, 2016.

500 Xuxin Cheng, Kexin Shi, Ananya Agarwal, and Deepak Pathak. Extreme parkour with legged robots. In *2024  
501 IEEE International Conference on Robotics and Automation (ICRA)*, pp. 11443–11450. IEEE, 2024.

502 Geoff Fink and Claudio Semini. Proprioceptive sensor fusion for quadruped robot state estimation. In *2020  
503 IEEE/RSJ International Conference on Intelligent Robots and Systems (IROS)*, pp. 10914–10920. IEEE,  
504 2020.

505 Noriaki Hirose, Amir Sadeghian, Marynel Vázquez, Patrick Goebel, and Silvio Savarese. Gonet: A semi-  
506 supervised deep learning approach for traversability estimation. In *2018 IEEE/RSJ international conference  
507 on intelligent robots and systems (IROS)*, pp. 3044–3051. IEEE, 2018.

508 Noriaki Hirose, Dhruv Shah, Ajay Sridhar, and Sergey Levine. Sacson: Scalable autonomous control for social  
509 navigation. *IEEE Robotics and Automation Letters*, 9(1):49–56, 2023.

510 David Hoeller, Nikita Rudin, Dhionis Sako, and Marco Hutter. Anymal parkour: Learning agile navigation for  
511 quadrupedal robots. *Science Robotics*, 9(88):eadi7566, 2024.

512 Junjie Huang, Guan Huang, Zheng Zhu, Yun Ye, and Dalong Du. Bevdet: High-performance multi-camera 3d  
513 object detection in bird-eye-view. *arXiv preprint arXiv:2112.11790*, 2021.

514 Haresh Karnan, Anirudh Nair, Xuesu Xiao, Garrett Warnell, Sören Pirk, Alexander Toshev, Justin Hart, Joydeep  
515 Biswas, and Peter Stone. Socially compliant navigation dataset (scand): A large-scale dataset of demonstra-  
516 tions for social navigation. *IEEE Robotics and Automation Letters*, 7(4):11807–11814, 2022.

517 Alex H Lang, Sourabh Vora, Holger Caesar, Lubing Zhou, Jiong Yang, and Oscar Beijbom. Pointpillars: Fast  
518 encoders for object detection from point clouds. In *Proceedings of the IEEE/CVF conference on computer  
519 vision and pattern recognition*, pp. 12697–12705, 2019.

520 Joonho Lee, Jemin Hwangbo, Lorenz Wellhausen, Vladlen Koltun, and Marco Hutter. Learning quadrupedal  
521 locomotion over challenging terrain. *Science robotics*, 5(47):eabc5986, 2020.

522 Zhiqi Li, Wenhui Wang, Hongyang Li, Enze Xie, Chonghao Sima, Tong Lu, Yu Qiao, and Jifeng Dai. Bev-  
523 former: Learning bird’s-eye-view representation from multi-camera images via spatiotemporal transformers.  
524 In *European conference on computer vision*, pp. 1–18. Springer, 2022.

525 Zhiqi Li, Zhiding Yu, David Austin, Mingsheng Fang, Shiyi Lan, Jan Kautz, and Jose M Alvarez. Fb-occ: 3d  
526 occupancy prediction based on forward-backward view transformation. *arXiv preprint arXiv:2307.01492*,  
527 2023.

528 Jing Liang, Dibyendu Das, Daeun Song, Md Nahid Hasan Shuvo, Mohammad Durrani, Karthik Taranath, Ivan  
529 Penskiy, Dinesh Manocha, and Xuesu Xiao. Gnd: Global navigation dataset with multi-modal perception  
530 and multi-category traversability in outdoor campus environments. *arXiv preprint arXiv:2409.14262*, 2024.

531 Tzu-Yuan Lin, Tingjun Li, Wenzhe Tong, and Maani Ghaffari. Proprioceptive invariant robot state estimation.  
532 *arXiv preprint arXiv:2311.04320*, 2023.

533 Haisong Liu, Haiguang Wang, Yang Chen, Zetong Yang, Jia Zeng, Li Chen, and Limin Wang. Fully sparse 3d  
534 panoptic occupancy prediction. *arXiv preprint arXiv:2312.17118*, 2023.

535 Zhijian Liu, Haotian Tang, Alexander Amini, Xinyu Yang, Huizi Mao, Daniela Rus, and Song Han. Bevfusion:  
536 Multi-task multi-sensor fusion with unified bird’s-eye view representation. *arXiv preprint arXiv:2205.13542*,  
537 2022.

540 Kai Luo, Hao Shi, Sheng Wu, Fei Teng, Mengfei Duan, Chang Huang, Yuhang Wang, Kaiwei Wang, and  
 541 Kailun Yang. Omnidirectional multi-object tracking. In *Proceedings of the Computer Vision and Pattern*  
 542 *Recognition Conference*, pp. 21959–21969, 2025.

543 Roberto Martin, Mihir Patel, Hamid Rezatofighi, Abhijeet Shenoi, JunYoung Gwak, Eric Frankel, Amir  
 544 Sadeghian, and Silvio Savarese. Jrdb: A dataset and benchmark of egocentric robot visual perception of  
 545 humans in built environments. *IEEE transactions on pattern analysis and machine intelligence*, 45(6):  
 546 6748–6765, 2021.

547 Takahiro Miki, Joonho Lee, Jemin Hwangbo, Lorenz Wellhausen, Vladlen Koltun, and Marco Hutter. Learning  
 548 robust perceptive locomotion for quadrupedal robots in the wild. *Science robotics*, 7(62):eabk2822, 2022.

549

550 Minho Oh, Byeongho Yu, I Nahrendra, Seoyeon Jang, Hyeonwoo Lee, Dongkyu Lee, Seungjae Lee, Yeeun  
 551 Kim, Marsim Kevin Christiansen, Hyungtae Lim, et al. Trip: Terrain traversability mapping with risk-aware  
 552 prediction for enhanced online quadrupedal robot navigation. *arXiv preprint arXiv:2411.17134*, 2024.

553 Jonah Philion and Sanja Fidler. Lift, splat, shoot: Encoding images from arbitrary camera rigs by implicitly  
 554 unprojecting to 3d. In *Computer Vision–ECCV 2020: 16th European Conference, Glasgow, UK, August*  
 555 *23–28, 2020, Proceedings, Part XIV 16*, pp. 194–210. Springer, 2020.

556

557 Fabio A Ruetz, Nicholas Lawrence, Emili Hernández, Paulo VK Borges, and Thierry Peynot. Foresttrav: 3d  
 558 lidar-only forest traversability estimation for autonomous ground vehicles. *IEEE Access*, 12:37192–37206,  
 559 2024.

560 Hilton Marques Souza Santana, João Carlos Virgolino Soares, Ylenia Nisticò, Marco Antonio Meggiolaro, and  
 561 Claudio Semini. Proprioceptive state estimation for quadruped robots using invariant kalman filtering and  
 562 scale-variant robust cost functions. In *2024 IEEE-RAS 23rd International Conference on Humanoid Robots*  
 563 (*Humanoids*), pp. 213–220. IEEE, 2024.

564 Amirreza Shaban, Xiangyun Meng, JoonHo Lee, Byron Boots, and Dieter Fox. Semantic terrain classification  
 565 for off-road autonomous driving. In *Conference on Robot Learning*, pp. 619–629. PMLR, 2022.

566 Dhruv Shah, Benjamin Eysenbach, Gregory Kahn, Nicholas Rhinehart, and Sergey Levine. Rapid exploration  
 567 for open-world navigation with latent goal models. *arXiv preprint arXiv:2104.05859*, 2021.

568

569 Dhruv Shah et al. ViKiNG: Vision-Based Kilometer-Scale Navigation with Geographic Hints. In *Proceedings*  
 570 *of Robotics: Science and Systems*, 2022. URL <http://www.robotsproceedings.org/rss18/p019.html>.

571 Haojie Shi, Qingxu Zhu, Lei Han, Wanchao Chi, Tingguang Li, and Max Q-H Meng. Terrain-aware  
 572 quadrupedal locomotion via reinforcement learning. *arXiv preprint arXiv:2310.04675*, 2023.

573

574 Pei Sun, Henrik Kretzschmar, Xerxes Dotiwalla, Aurelien Chouard, Vijaysai Patnaik, Paul Tsui, James Guo,  
 575 Yin Zhou, Yuning Chai, Benjamin Caine, et al. Scalability in perception for autonomous driving: Waymo  
 576 open dataset. In *Proceedings of the IEEE/CVF conference on computer vision and pattern recognition*, pp.  
 2446–2454, 2020.

577

578 Xiaoyu Tian, Tao Jiang, Longfei Yun, Yucheng Mao, Huitong Yang, Yue Wang, Yilun Wang, and Hang Zhao.  
 579 Occ3d: A large-scale 3d occupancy prediction benchmark for autonomous driving. *Advances in Neural*  
 580 *Information Processing Systems*, 36:64318–64330, 2023.

581

582 Wenwen Tong, Chonghao Sima, Tai Wang, Li Chen, Silei Wu, Hanming Deng, Yi Gu, Lewei Lu, Ping Luo,  
 583 Dahua Lin, et al. Scene as occupancy. In *Proceedings of the IEEE/CVF International Conference on*  
 584 *Computer Vision*, pp. 8406–8415, 2023.

585

586 Unitree. Unitree go2-w product page, 2025-07-27. <https://www.unitree.com/go2-w>.

587

588 Allan Wang, Daisuke Sato, Yasser Corzo, Sonya Simkin, Abhijat Biswas, and Aaron Steinfeld. Tbd pedestrian  
 589 data collection: Towards rich, portable, and large-scale natural pedestrian data. In *2024 IEEE International*  
 590 *Conference on Robotics and Automation (ICRA)*, pp. 637–644. IEEE, 2024.

591

592 Mingkun Wang, Xinge Zhu, Changqian Yu, Wei Li, Yuexin Ma, Ruochun Jin, Xiaoguang Ren, Dongchun  
 593 Ren, Mingxu Wang, and Wenjing Yang. Ganet: Goal area network for motion forecasting. *arXiv preprint*  
 594 *arXiv:2209.09723*, 2022.

595

596 Benjamin Wilson, William Qi, Tanmay Agarwal, John Lambert, Jagjeet Singh, Siddhesh Khandelwal, Bowen  
 597 Pan, Ratnesh Kumar, Andrew Hartnett, Jhony Kaezemel Pontes, et al. Argoverse 2: Next generation  
 598 datasets for self-driving perception and forecasting. *arXiv preprint arXiv:2301.00493*, 2023.

594 Pengchuan Xiao, Zhenlei Shao, Steven Hao, Zishuo Zhang, Xiaolin Chai, Judy Jiao, Zesong Li, Jian Wu, Kai  
 595 Sun, Kun Jiang, et al. Pandaset: Advanced sensor suite dataset for autonomous driving. In *2021 IEEE*  
 596 *international intelligent transportation systems conference (ITSC)*, pp. 3095–3101. IEEE, 2021.

597 Zhi Yan, Li Sun, Tom Duckett, and Nicola Bellotto. Multisensor online transfer learning for 3d lidar-based  
 598 human detection with a mobile robot. In *2018 IEEE/RSJ International Conference on Intelligent Robots and*  
 599 *Systems (IROS)*, pp. 7635–7640. IEEE, 2018.

600 Zhi Yan, Simon Schreiberhuber, Georg Halmetschlager, Tom Duckett, Markus Vincze, and Nicola Bellotto.  
 601 Robot perception of static and dynamic objects with an autonomous floor scrubber. *Intelligent Service*  
 602 *Robotics*, 13(3):403–417, 2020.

603 Zichen Yu, Changyong Shu, Jiajun Deng, Kangjie Lu, Zongdai Liu, Jiangyong Yu, Dawei Yang, Hui Li, and  
 604 Yan Chen. Flashocc: Fast and memory-efficient occupancy prediction via channel-to-height plugin. *arXiv*  
 605 *preprint arXiv:2311.12058*, 2023.

606 Arthur Zhang, Chaitanya Eranki, Christina Zhang, Ji-Hwan Park, Raymond Hong, Pranav Kalyani, Lochana  
 607 Kalyanaraman, Arsh Gamaare, Arnav Bagad, Maria Esteva, et al. Toward robust robot 3-d perception in urban  
 608 environments: The ut campus object dataset. *IEEE Transactions on Robotics*, 40:3322–3340, 2024.

609 Yifu Zhang, Peize Sun, Yi Jiang, Dongdong Yu, Fucheng Weng, Zehuan Yuan, Ping Luo, Wenyu Liu, and Xing-  
 610 gang Wang. Bytetrack: Multi-object tracking by associating every detection box. In *European conference*  
 611 *on computer vision*, pp. 1–21. Springer, 2022.

612 Yifu Zhang, Xinggang Wang, Xiaoqing Ye, Wei Zhang, Jincheng Lu, Xiao Tan, Errui Ding, Peize Sun, and  
 613 Jingdong Wang. Bytetrackv2: 2d and 3d multi-object tracking by associating every detection box, 2023.  
 614 URL <https://arxiv.org/abs/2303.15334>.

615 Zhengyou Zhang. Flexible camera calibration by viewing a plane from unknown orientations. In *Proceedings*  
 616 *of the seventh ieee international conference on computer vision*, volume 1, pp. 666–673. Ieee, 1999.

617 Fangcheng Zhu, Yunfan Ren, and Fu Zhang. Robust real-time lidar-inertial initialization. In *2022 IEEE/RSJ*  
 618 *International Conference on Intelligent Robots and Systems (IROS)*, pp. 3948–3955. IEEE, 2022.

619 Shifan Zhu et al. Cear: Comprehensive event camera dataset for rapid perception of agile quadruped robots.  
 620 *IEEE Robotics and Automation Letters*, 2024.

621

622

623

624

625

626

627

628

629

630

631

632

633

634

635

636

637

638

639

640

641

642

643

644

645

646

647